HIGH-EFFICIENCY AMORPHOUS SILICON AND NANOCRYSTALLINE SILICON BASED SOLAR CELLS AND MODULES

Quarterly Technical Progress Report
August 1 through October 31, 2006

S. Guha and J. Yang
United Solar Ovonic LLC
Troy, Michigan

NREL Technical Monitor: Bolko von Roedern

Prepared under Subcontract No. ZXL-6-44205-14

Table of Contents

Preface

This Quarterly Report covers the work performed by United Solar Ovonic LLC under the Thin Film Partnership Subcontract No. ZXL-6-44205-14 for the period from August 1, 2006 to October 31, 2006. The following personnel participated in this research program.

A. Banerjee, E. Chen, G. Fischer, S. Guha (Principal Investigator), B. Hang, M. Hopson, A. Mohsin, J. Noch, J. M. Owens, T. Palmer, L. M. Sivec, D. Wolf, B. Yan, J. Yang (Co-Principal Investigator), K. Younan, and G. Yue.

Collaboration with National Renewable Energy Laboratory is acknowledged.

1. nc-Si:H solar cells with different thicknesses of the intrinsic and *i/p* buffer layers

1. 1. Introduction

Hydrogenated nanocrystalline silicon (nc-Si:H) as a novel solar cell material shows a number of different behaviors from its hydrogenated amorphous silicon (a-Si:H) counterpart. We previously reported [1] that as the intrinsic layer thickness increases, the open circuit voltage (V_{oc}) drops more significantly in nc-Si:H cells than in a-Si:H cells. We attributed this to the fact that the crystalline volume fraction increases with increasing thickness. We also found that the nc-Si:H cell performance strongly depends on the *i/p* buffer layer [2]. Without a proper buffer layer, the nc-Si:H cell shows a poorer fill factor (FF) and a smaller V_{oc}, which, in turn, leads to a low conversion efficiency. Recently, we found that the behaviors of metastability after prolonged light soaking in nc-Si:H solar cells are different from a-Si:H cells in many cases. First, we observed no light-induced degradation when the photon energy is lower than the bandgap of a-Si:H. However, light-induced degradation occurs when the photon energy is greater than the a-Si:H bandgap. We conclude that the light-induced defect generation occurs mainly in the amorphous phase or in the grain boundary regions [3]. Second, a forward current injection doesn't degrade the nc-Si:H cell performance, which is contrary to a-Si:H cells. Third, a reverse electrical bias during light soaking enhances the degradation [4, 5], which is also contrary to a-Si:H solar cells. Fourth, the nc-Si:H cells made with an optimized hydrogen dilution profile show minimal light-induced degradation although these cells have a high amorphous volume fraction [6]. This indicates that the amorphous volume fraction is not the only factor determining the light-induced degradation. Other factors, such as the structure and distribution of the amorphous component, as well as the properties of the grain boundaries, may play important roles in the nc-Si:H stability.

In this quarter, we carried out a systematic study of the effects of the intrinsic and *i/p* buffer layer thicknesses on nc-Si:H cell performance and stability. To avoid the microstructure evolution with thickness as mentioned before, the hydrogen dilution profiling technique [7] has been used so that the intrinsic layers in all the cells maintain similar crystalline volume fraction along the growth direction. The results show that both the cell performance and the stability are related to the intrinsic and *i/p* buffer layer thicknesses.

1. 2. Experimental details

nc-Si:H *n-i-p* single-junction solar cells were deposited using a multi-chamber glow discharge system with RF chambers for the doped layers and a modified very high frequency (MVHF) chamber for the intrinsic layers at a deposition rate of ~ 3-5 Å/s. The same hydrogen dilution profile was used for all of the intrinsic layer depositions. The same *n/i* buffer and seeding layers were used for all the samples. The samples with different intrinsic layer thicknesses were made by controlling intrinsic layer deposition time. The a-Si:H *i/p* buffers were made with RF glow discharge at a deposition rate of ~ 1 Å/s. For comparison, high rate a-Si:H cells with different intrinsic layer thicknesses were also made with MVHF at a deposition rate of ~ 6 Å/s. Both nc-Si:H and a-Si:H cells were deposited on Ag/ZnO coated stainless steel substrates. The current-density versus voltage (*J-V*) characteristics were measured under an AM1.5 solar simulator at 25 ^{o}C. Quantum efficiency (QE) spectra were measured from 300 to

1000 nm under the short circuit condition at room temperature. The short circuit current density (J_{sc}) was calculated by the integral of quantum efficiency (QE) with the AM1.5 spectrum. The material structure of the intrinsic layer was directly measured on the cells with no *i/p* buffer layer using Raman spectroscopy with a green light (532 nm) excitation. Light soaking was carried out under 100 mW/cm^2 of white light at 50 ^{o}C under the open circuit condition for 1000 hours. Dark *J-V* characteristics of the cells were measured in a vacuum chamber using a programmable multi-meter at a controlled temperature.

1. 3. Results and discussion

Table I lists the *J-V* characteristics of nine nc-Si:H single-junction solar cells with different intrinsic and *i/p* buffer layer thicknesses. The same hydrogen dilution profile was used for all the nc-Si:H intrinsic layer depositions. The different intrinsic layer thicknesses were obtained by simply controlling deposition time as listed in column 2. For each intrinsic layer thickness, three different thicknesses of a-Si:H *i/p* buffers with the deposition times of 0, 3, and 7 minutes (corresponding to thicknesses of 0, 180, and 420 Å) were added to study the effect of buffer layer thickness. From Table I, the following observations are made. First, for the effect of the intrinsic layer thickness, we found that the fill factor (FF) decreases, and the J_{sc} increases with increasing the intrinsic layer thickness. The V_{oc} does not change too much with the intrinsic layer thickness for the cells with zero and 3-minute *i/p* buffer layers. However, for the cells with a 7-minute *i/p* buffer layer, the V_{oc} decreases noticeably with an increase in the intrinsic layer thickness. Alao, the conversion efficiency increases with the intrinsic layer thickness. Second, for the effect of the *i/p* buffer layer thickness, three points have been identified. First, the V_{oc} increases with increasing *i/p* buffer layer thickness. Second, the FF does not improve by adding the *i/p* buffer layer. For the thin cells, the FF is even reduced. Third, the *i/p* buffer layer has a greater effect on the thin cells than the thick ones. For example, when the *i/p* buffer layer thickness was increased from 0 to 7 minutes the V_{oc} increased from 0.463 to 0.532 V for the cells with a 7-minute intrinsic layer, which is significantly larger than the increase from 0.455 to 0.483 V for the cells with a 30-minute intrinsic layer. This phenomenon is even more pronounced in the FF. For the cells with a 7-minute intrinsic layer, the FF is reduced from 0.714 to 0.677 when

Table I. *J-V* characteristics of nine nc-Si:H single-junction solar cells on Ag/ZnO substrate with different thicknesses of the intrinsic and *i/p* buffer layers.

Sample No.	Time (i) (min)	Time (i/p) (min)	V_{oc} (V)	FF	J_{sc} (mA/cm^2)	P_{max} (mW/cm^2)
14098	7	0	0.463	0.714	14.54	4.81
14099	15	0	0.455	0.641	18.71	5.46
14100	30	0	0.455	0.586	22.49	6.00
14101	7	3	0.481	0.700	14.18	4.77
14111	15	3	0.473	0.642	18.78	5.70
14112	30	3	0.473	0.590	22.87	6.38
14113	7	7	0.532	0.677	16.00	5.76
14114	15	7	0.491	0.622	19.73	6.03
14106	30	7	0.483	0.590	22.82	6.50

Table II. Deconvolution results of the Raman spectra, where A, P, W, and H denote the area, peak position, width, and height of each deconvolution component, respectively. R represents the ratio of the areas of the c-Si and intermediate peaks to the total areas of the three peaks.

Sample No.	amorphous				intermediate				crystalline				R
	A	P	W	H	A	P	W	H	A	P	W	H	
14098	18.1	481	86	0.2	6.2	505	29	0.2	9.6	520	11	0.7	46.6%
14099	12.7	479	70	0.2	6.9	507	29	0.2	9.8	520	13	0.8	56.8%
14100	10.8	478	69	0.2	6.8	507	29	0.2	10.0	520	13	0.8	60.9%

the *i/p* buffer layer is increased from 0 to 7 minutes. However, for the cells with a 30-minute intrinsic layer, the FF is not sensitive to the *i/p* buffer layer thickness.

As mentioned previously, to control the effect of microstructure evolution on the cell performance, we have used the hydrogen dilution profiling technique in the intrinsic layer deposition to keep the crystalline volume fraction constant in the material along the growth direction. To confirm this, Raman spectroscopy measurements were made on the cells with different intrinsic layer thicknesses by using a green laser excitation (wavelength=532 nm). In order to avoid the potential influence of the a-Si:H *i/p* buffer on measurement results, the cells with no *i/p* buffer layer (samples 14098, 14099, 14100) were selected for the Raman measurements. Figure 1 (a) shows the Raman spectra for the three samples. One can clearly see that the three cells have very similar crystalline volume fractions. For a detailed analysis, we deconvoluted the Raman spectra into three components of amorphous TO (~ 480 cm^{-1}), intermediate (~ 500 cm^{-1}), and crystalline (~520 cm^{-1}) modes using three Gaussian functions as shown in Fig. 1 (b). The results are summarized in Table II. The crystalline volume fraction listed in the table is simply defined as the ratio of the areas of the crystalline and the intermediate modes to the total. The crystalline volume fractions for the cells with 7, 15, and 30 minutes of intrinsic layers are 46.6%, 56.8%, and 60.9%, respectively. We noted that the volume fraction in the thicker cell is still slightly higher than in the thinner one.

Dark *J-V* measurement is a powerful tool in studying the recombination mechanism in a-Si:H based solar cells. An ideal solar cell follows the typical diode characteristics of $J=J_0[exp(qV/nKT)-1]$, where J_0 is the reverse saturated current density, q the unit charge, T the measurement temperature, k the Boltzmann constant, and n the diode quality factor. By studying the dark *J-V* and examining the deviation of experimental results from the diode characteristics, one can examine the shunt current and the recombination mechanism of the carriers in the solar cells. In this study, we used the dark *J-V* measurement to study the nine nc-Si:H solar cells. The results are plotted in Fig. 2. One can see that the dark current density reduces with the increased *i/p* buffer layer thickness. The cells with a thinner intrinsic layer show a larger reduction in the dark current density. Moreover, we found that the cells with no *i/p* buffer layer have a high shunt current density. With the *i/p* buffer layer thickness increased, the shunt current density is continually reduced.

For the cells with a 7-minute *i/p* buffer, the shunt current density becomes minimized and the dark *J-V* curves basically follow the diode characteristics as shown in Fig. 2 (d). By fitting the data of these three samples with the diode characteristics, we obtained the reverse saturated currents (J_0) and the diode quality factors (n), as listed in Table III. One can see that the diode quality factors are very similar, which means that the carrier recombination mechanism is the same for the samples. The saturated current is increased by increasing the thickness of the

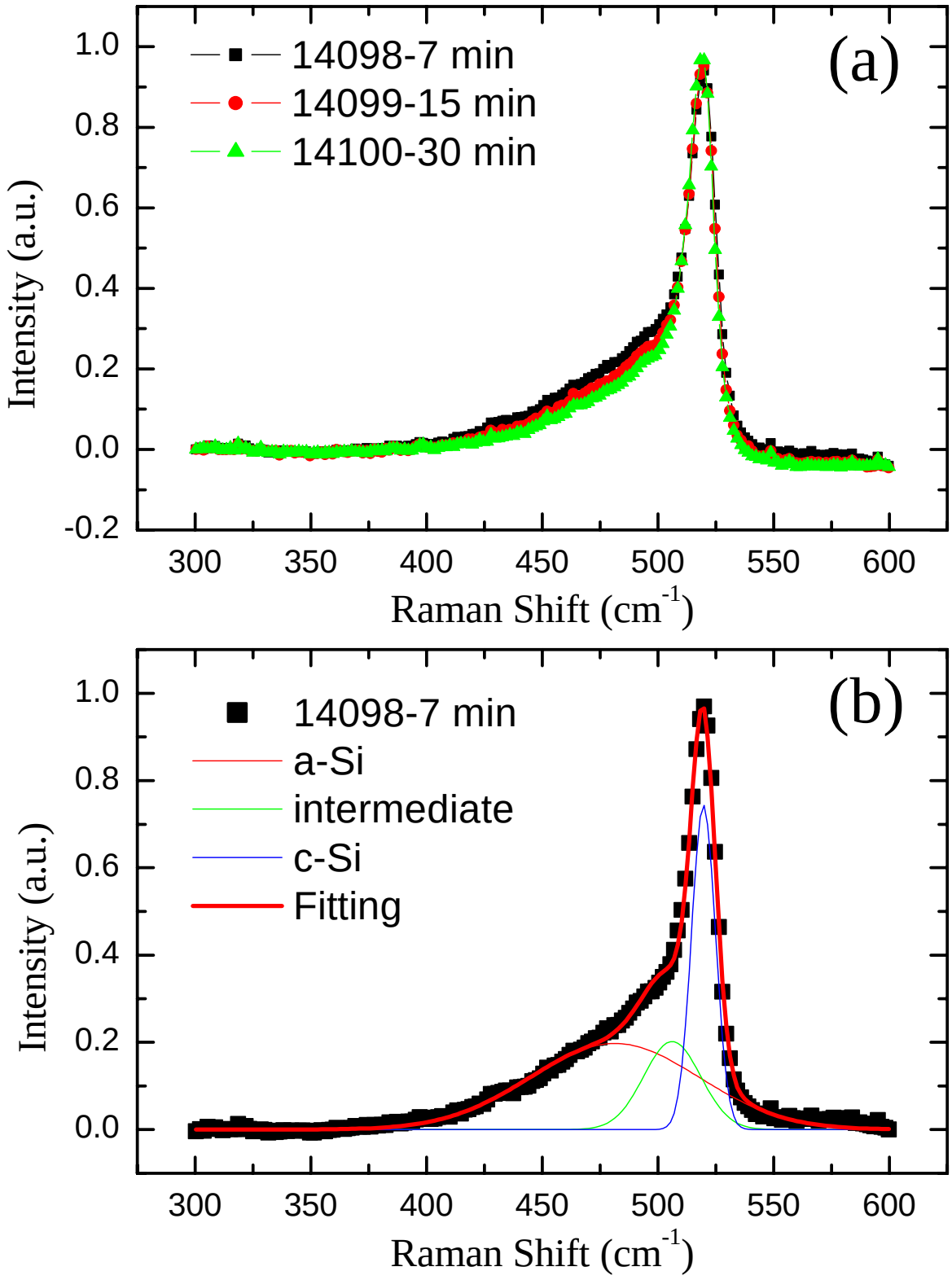

Figure 1. (a) Comparison of Raman spectra for the samples with different intrinsic thicknesses and with no i/p buffer, (b) an example of a Raman spectrum deconvolution.

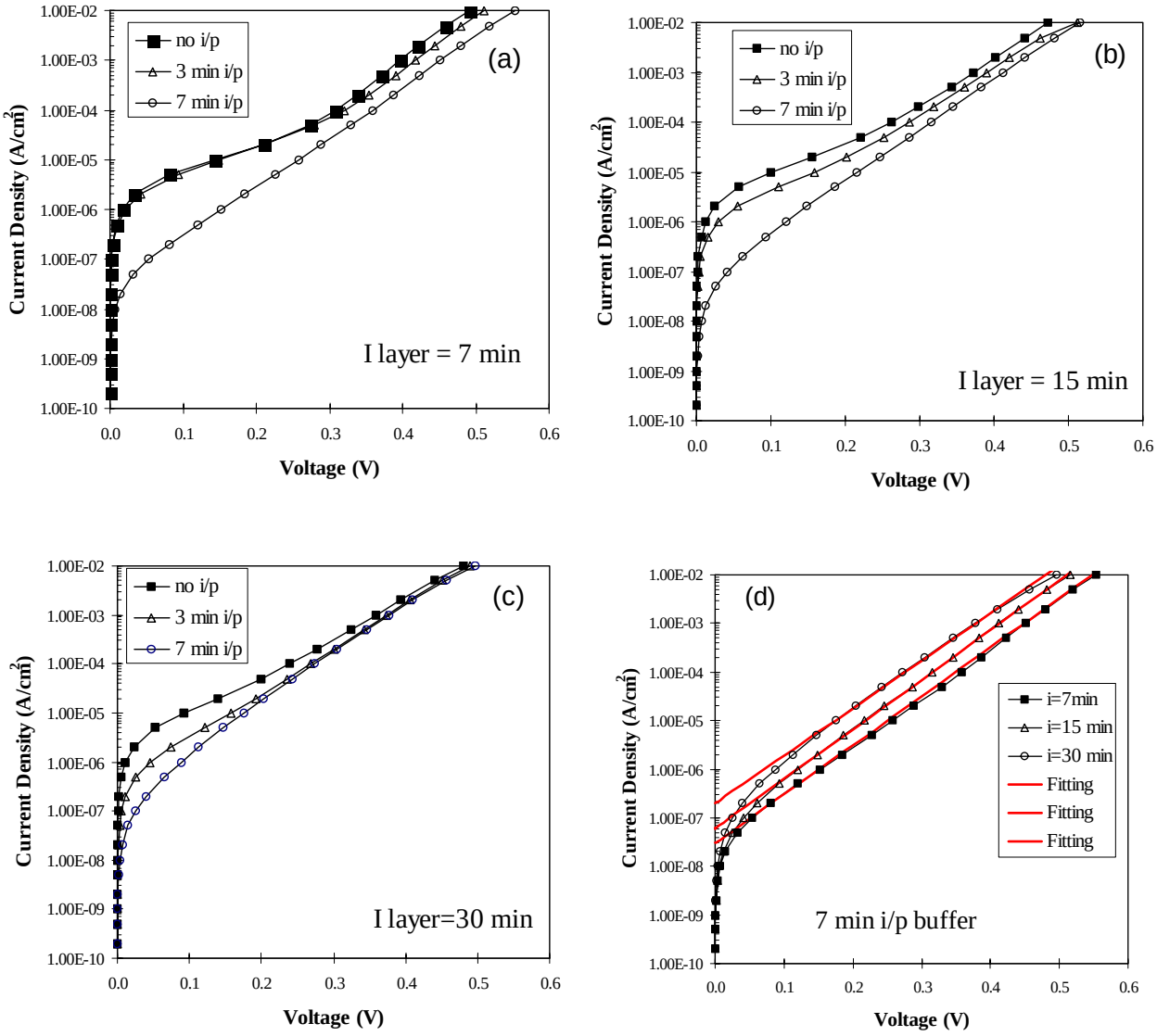

Figure 2. Dark *J-V* characteristics of the cells with (a) a 7-minute intrinsic layer but with different *i/p* buffer thicknesses; (b) a 15-minute intrinsic layer but with different *i/p* buffer layer thicknesses; (c) 30-minute intrinsic layer but with different *i/p* buffers; (d) different intrinsic layer thicknesses but with the same *i/p* buffer layer thickness of 7 minutes.

Table III. The dark J-V fitting results of three nc-Si:H cells with different intrinsic layer thicknesses. The *i/p* buffer layer is the same for the samples (7 minutes). J_0 denotes the reverse saturated current, and *n* the diode quality factor.

Sample No.	*i* layer deposition time	J_0 (A/cm^2)	*n*
14113	7 min	3×10^{-8}	1.75
14114	15 min	6×10^{-8}	1.67
14106	30 min	2×10^{-7}	1.70

intrinsic layer, indicating a greater recombination rate in the thicker samples. Previously, we found that thedark *J-V* characteristics of a-Si:H solar cells are largely independent of the intrinsic layer thickness. This phenomenon could be explained with a weak thickness dependence of the recombination width, which is smaller than the intrinsic layer thickness. However, in the nc-Si:H solar cells, the dark *J-V*, especially the J_0, strongly depends on the intrinsic layer thickness. A thicker intrinsic layer results in a larger J_0, which could indicate that the recombination width is the same as the intrinsic layer thickness. A time-of-flight measurement found that the hole mobility in nc-Si:H is over one hundred times larger than in a-Si:H [8]. Correspondingly, the hole diffusion length in nc-Si:H solar cells is much larger than in a-Si:H solar cells and the improved hole diffusion length leads to a recombination width similar to the intrinsic layer thickness.

We now discuss the main points obtained from the experimental results. First, we know that the FF usually decreases with an increase in the intrinsic layer thickness because of the reduction of built-in electric field and increased recombination rate. The intrinsic layer thickness dependence of FF in the nine samples follows this common trend. It is also understandable that the J_{sc} increases with increased intrinsic layer thickness since the light absorption is increased. Here, we need to point out that this is true for the cells with a certain thickness range. Beyond this range, other factors such as microstructure evolution, carrier collection length, or collapse of the built-in electric field, might play dominant roles. Compared to the FF and J_{sc}, the effect of intrinsic layer thickness on the V_{oc} is more complicated. Previously, we found that the V_{oc} reduces with increasing thickness more dramatically in nc-Si:H than in a-Si:H solar cells [1]. One explanation was the evolution of crystalline volume fraction with the intrinsic layer thickness. A similar trend is also observed in these nine samples as listed in Table I. The reason for a small V_{oc} change with the intrinsic layer thickness for the cells with no or thin *i/p* buffer is probably due to the large shunt current density or a large recombination current density in the *i/p* interface. This is consistent with the results from dark *J-V* measurements. With the increase of the *i/p* buffer layer thickness to 7 minutes, the shunt-current or interface recombination current was reduced, and the V_{oc} monotonically decreased with the intrinsic layer thickness. Moreover, from the Raman measurements, we noticed that the increase of crystalline volume fraction with the intrinsic layer thickness is small, which could not be the dominant factor for the reduced V_{oc} in the thicker cells. Instead, the significantly increased dark current density could be the main reason for the reduced V_{oc} in the thicker cells. Second, we found that the V_{oc} increases with increasing the *i/p* buffer layer thickness. This is simply because the a-Si:H *i/p* buffer layer reduces the shunt current density. This was confirmed by the dark *J-V* measurements as shown in Figure 2 (a), (b), and (c). We know that, in the light *J-V* measurement, the V_{oc} is obtained

when the dark current equals photo current. The larger the dark current is, the smaller the V_{oc}. We also found that the FF is not improved for these cells when the buffer layer was added. This is probably because the a-Si:H *i/p* buffer is too thick and introduces an extra series resistance. Another interesting observation is that the *i/p* buffer has a larger effect on the thin cells than thick ones. It may indicate that the cell performance of the thin samples was dominated by the *i/p* interface, while the performance of the thick samples was dominated by the bulk properties.

A stability study has been carried out on the nine nc-Si:H solar cells, and the results are listed in Table IV. As a comparison, four high rate a-Si:H solar cells with different intrinsic layer thicknesses were also studied, and the results are listed in Table V. Three points have been observed from the tables. First, the light-induced degradation rate in nc-Si:H decreases with increasing the intrinsic layer thickness. This is different from the case in a-Si:H based solar cells, where we usually found that the degradation rate increases with the intrinsic layer

Table IV. Stability results of nc-Si:H solar cells with different intrinsic and *i/p* buffer layer thicknesses.

Sample No.	Time (i) (min)	Time(i/p) (min)	Status	V_{oc} (V)	FF	Q (mA/cm^2)	P_{max} (mW/cm^2)
14098	7	0	Initial	0.463	0.714	14.54	4.81
			Stable	0.422	0.672	14.60	4.14
			Deg.(%)	-8.9%	-5.9%	0	-13.9%
14099	15	0	Initial	0.455	0.641	18.71	5.46
			Stable	0.433	0.641	18.90	5.25
			Deg.(%)	-4.8%	0	+1.0%	-4.0%
14100	30	0	Initial	0.455	0.586	22.49	6.00
			Stable	0.443	0.586	22.83	5.93
			Deg.(%)	-2.6%	0	+1.5%	-1.2%
14101	7	3	Initial	0.481	0.700	14.18	4.77
			Stable	0.462	0.673	14.57	4.53
			Deg.(%)	-4.0%	-3.9%	+2.8%	-5.0%
14111	15	3	Initial	0.473	0.642	18.78	5.70
			Stable	0.448	0.646	18.92	5.48
			Deg.(%)	-5.3%	+0.6%	+0.7%	-3.9%
14112	30	3	Initial	0.473	0.590	22.87	6.38
			Stable	0.459	0.597	22.91	6.28
			Deg.(%)	-3.0%	+1.2%	+0.2%	-1.6%
14113	7	7	Initial	0.532	0.677	16.00	5.76
			Stable	0.516	0.679	16.04	5.62
			Deg.(%)	-3.0%	0	0	-2.4%
14114	15	7	Initial	0.491	0.622	19.73	6.03
			Stable	0.492	0.646	19.51	6.20
			Deg.(%)	0	+3.9%	-1.1%	+2.8%
14106	30	7	Initial	0.483	0.590	22.82	6.50
			Stable	0.481	0.597	22.62	6.50
			Deg.(%)	0	+1.2%	-0.9%	0

thickness. Second, adding an *i/p* buffer layer reduces the degradation rate, especially for the thin solar cells. For example, sample 14098 with no *i/p* buffer degrades ~14% in efficiency, whereas sample 14113 with a 7-minute *i/p* buffer layer degrades only ~ 2%. However, for the thick samples, the degradation rate does not change much when the *i/p* buffer layer is changed, which can be seen by comparing sample 14100 with no *i/p* buffer and sample 14106 with a 7-minute *i/p* buffer layer. To clearly see this trend, we plotted the degradation rate versus the intrinsic layer thickness in Fig. 3. Third, the degradation (if any) happens mostly in V_{oc} and FF. J_{sc} shows almost no degradation for all the samples.

As discussed above, the cell performance in thin cells is mainly dominated by the *i/p* interface. Since light soaking causes more damage in the *i/p* interface than in the bulk due to more exposure, the thin cells will be subjected to more degradation than the thick cells. Moreover, according to our experience, the V_{oc} and FF are more sensitive to the *i/p* interface than J_{sc}. Any change in the *i/p* interface will be reflected in V_{oc} and FF first. This is in agreement with the observation in the third point. Improving the interface by adding high quality amorphous *i/p* buffer should also reduce the light-induced degradation in the *i/p* interface region. This explains why adding an *i/p* buffer layer reduces the degradation rate. Previously, it has been reported that the bulk properties are improved by using a hydrogen dilution profiling technique [7], but actually the main improvement occurs close to the *i/p* interface region due to decreased hydrogen dilution. Based on the same argument, it is not surprising that the thick cells with an optimized *i/p* buffer have very stable performance.

The dark *J-V* characteristics of the nine nc-Si:H solar cells after light soaking are plotted in Fig. 4. Compared to the corresponding initial results, all dark *J-V* curves are shifted upward, indicating an enhanced recombination rate after light-soaking. It is noticed that a larger V_{oc} decrease corresponds to a larger dark current increase. For the cells with a thicker *i/p* buffer (7-minute *i/p* buffer), the curves are shifted in parallel. However, for the cells with no *i/p* buffer, the shunt current (low voltage part) does not change. Only the recombination current (high voltage part) increased after light soaking as seen in Fig. 4 (a).

Table V. Stability results of high rate a-Si:H solar cells with different intrinsic layer thicknesses. The cells were deposited using MVHF on Ag/ZnO coated stainless steel substrates.

Sample No.	Status	Q (mA/cm^2)	V_{oc} (V)	FF	P_{max} (mW/cm^2)	Thickness (nm)
14672	Initial	9.12	1.021	0.755	7.03	104
	Stable	8.93	0.977	0.711	6.20	
	Deg.	2.1%	4.3%	5.8%	11.8%	
14671	Initial	11.11	0.987	0.744	8.16	156
	Stable	10.77	0.970	0.690	7.21	
	Deg.	3.1%	1.7%	7.3%	11.6%	
14673	Initial	12.87	0.999	0.716	9.21	235
	Stable	12.32	0.973	0.666	7.98	
	Deg.	4.3%	2.6%	7.0%	13.4%	
14674	Initial	13.77	1.001	0.690	9.51	307
	Stable	12.97	0.973	0.632	7.98	
	Deg.	5.8%	2.8%	8.4%	16.1%	

1. 4. Summary

In summary, the effects of the intrinsic and *i/p* buffer layer thicknesses on nc-Si:H cell performance and stability have been studied. The results show that the *i/p* buffer layer not only has a large effect on cell performance, but also on the stability. For the cells with a thin intrinsic layer, the cell performance, especially V_{oc}, is limited by the *i/p* interface. An optimized *i/p* buffer layer can improve the cell performance significantly. For the thick cells, the cell performance is limited by the bulk properties of the intrinsic layer. In this case, the buffer layer effect becomes less obvious. We also found that the stability dependence on intrinsic layer thickness for nc-Si:H cells is different from a-Si:H cells. The results were explained in terms of different contributions from the bulk properties of the intrinsic layer and the *i/p* interface layer.

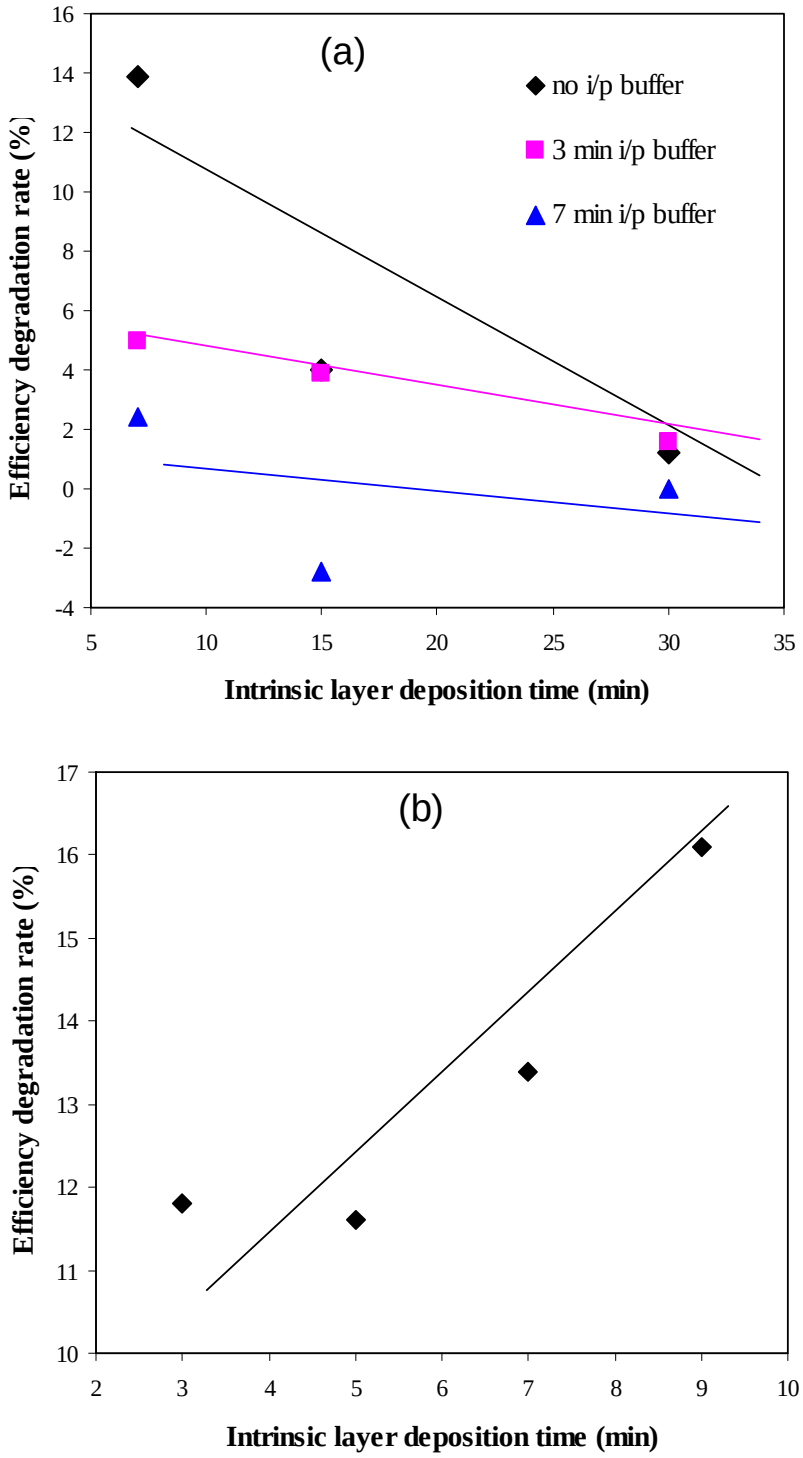

Figure 3. (a) Efficiency degradation rate as a function of intrinsic layer deposition time in nc-Si:H solar cells. The thicknesses are in the range of 350 to 900 nm; (b) Efficiency degradation rate as a function of intrinsic layer deposition time in a-Si:H solar cells. The thicknesses are in the range of 100 to 300 nm.

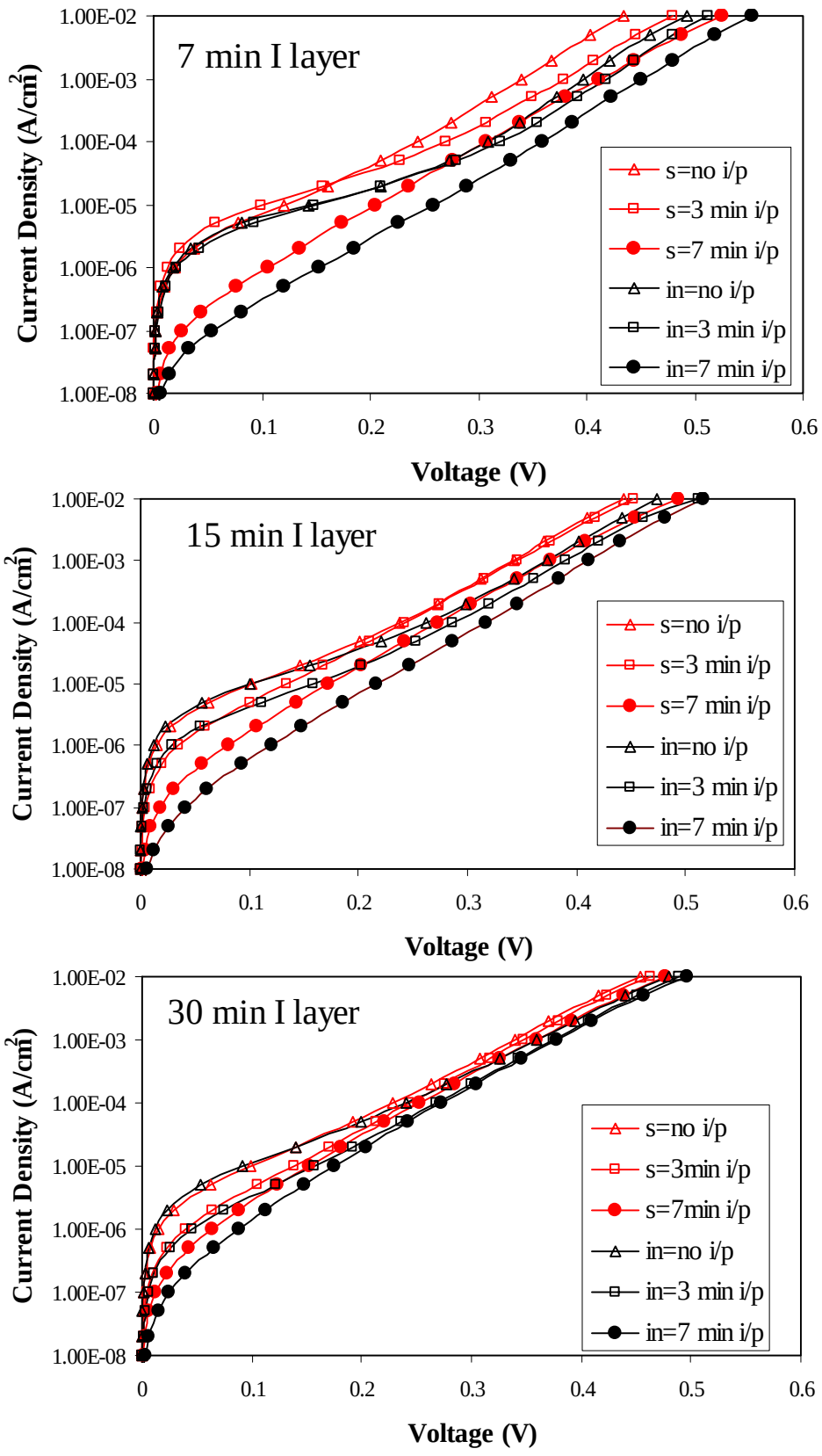

Figure 4. Dark *J-V* characteristics of nine nc-Si:H cells before and after light-soaking. Initial state is denoted by "in", and stabilized state is denoted by "s".

2. High rate deposition of a-SiGe:H component cells and a-Si:H/a-SiGe:H double-junction cells made using MVHF technique

2. 1. Introduction

In the last report, we reported that both initial performance and stability in the high rate a-Si:H solar cells made by MVHF are independent of the deposition rate in the range of 1-14 Å/s. Encouraged by this result, we proceeded to develop high rate a-SiGe:H component cells and a-Si:H/a-SiGe:H double-junction cells. By combining the optimized a-Si:H top and a-SiGe:H bottom cells, we achieved a 11.7% initial active-area efficiency with an a-Si:H/a-SiGe:H double-junction structure on Ag/ZnO coated SS substrate at a deposition rate of 10 Å/s in both intrinsic layers.

2. 2. High rate a-SiGe:H single-junction cells at a deposition rate of 10 Å/s

A series of a-SiGe:H *n-i-p* single-junction cells was made with a MVHF high rate a-SiGe:H intrinsic layer and RF doped layers on stainless steel substrates. The *n/i* and *i/p* buffer layers were made using RF at a low rate of ~1 Å/s. The deposition time of the a-SiGe:H intrinsic layer was fixed at 4 minutes, which corresponds to a deposition rate of ~ 10Å/s. ITO dots with an active area of 0.25 cm^2 were deposited on the *p* layer for *J-V* and QE measurements. The major techniques to optimize the recipe include: (1) a proper GeH_4 ramping to enhance hole collection, (2) an optimized *i/p* buffer to reduce shunt current and interface recombination, and (3) optimized *p* and *n* layers to reduce series resistance.

Table VI lists the *J-V* characteristics of typical a-SiGe:H component cells made at high rates. In this study, we focused on medium bandgap materials, which gives an AM1.5 V_{oc} around 0.75 to 0.80 V for high efficiency a-Si:H/a-SiGe:H double-junction cells. In order to investigate the long wavelength response and simulate the performance when the a-SiGe:H cell is placed into an a-Si:H/a-SiGe:H double-junction structure, we measured the cell performance under an AM1.5 solar simulator with a 530-nm cut on filter. From previous experience, a P_{max} of 4 mW/cm^2 is a benchmark for good a-SiGe:H component cells on stainless steel substrate. In this study, we achieved an active-area P_{max} of 4.4 mW/cm^2 under AM1.5 with a 530-nm cut-on filter. Figure 5 shows the *J-V* curves and QE spectrum of the optimized a-SiGe:H component cell.

Table VI. *J-V* characteristics of the typical a-SiGe:H component cells made with MVHF at high rates. The intrinsic layer deposition time for all the cells is 4 minutes. The results in parentheses were measured under AM1.5 with a 530 nm cut-on filter.

Sample No.	V_{oc} (> 530 nm) (V)	FF (> 530 nm)	J_{sc} (> 530 nm) (mA/cm^2)	P_{max} (> 530 nm) (mW/cm^2)
14407	0.795(0.775)	0.667(0.696)	13.49(7.82)	7.15(4.22)
14583	0.768(0.751)	0.648(0.671)	14.41(8.66)	7.17(4.36)
14584	0.768(0.750)	0.664(0.681)	14.23(8.60)	7.26(4.39)

2. 3. a-Si:H/a-SiGe:H double-junction solar cells made with MVHF at high rates

Having optimized the a-Si:H top and a-SiGe:H bottom cells, we proceeded to combine them to make a-Si:H/a-SiGe:H double-junction solar cells on Ag/ZnO coated stainless steel substrates. The deposition time in both the top and bottom cell intrinsic layers was fixed at 4 minutes. The *J-V* characteristics of typical double-junction cells are listed in Table VII. An initial active-area efficiency of 11.7% has been achieved. The *J-V* curves and QE spectra of the best a-Si:H/a-SiGe:H double-junction cell are plotted in Fig. 6.

2. 4. Summary

In summary, we have optimized the a-SiGe:H component cells at high deposition rates on SS substrate. An active-area P_{max} of 4.4 mW/cm^2 has been achieved under AM1.5 with a 530 nm cut-on filter. By combining this cell with an optimized high rate a-Si:H top cell, we have made an a-Si:H/a-SiGe:H double-junction cell on Ag/ZnO coated SS with an initial active-area efficiency of 11.7%.

Table VII. *J-V* characteristics of the a-Si:H/a-SiGe:H double-junction cells made at high rates. The deposition time in both top and middle cell intrinsic layers was 4 minutes.

Sample No.	V_{oc} (V)	FF	QE (mA/cm^2)			P_{max} (mW/cm^2)
			Top	Bottom	Total	
14520	1.719	0.717	9.50	10.94	20.44	11.71
14530	1.696	0.664	10.23	10.16	20.39	11.44
14534	1.700	0.679	9.78	10.48	20.26	11.29

References:

[1] B. Yan, G. Yue, J. Yang, A. Banerjee, and S. Guha, Mat. Res. Soc. Symp. Proc. **762**, 309 (2003).
[2] J. Yang, B. Yan, G. Yue, and S. Guha, 31st IEEE PVSC, 1359 (2005).
[3] B. Yan, G. Yue, J.M. Owens, J. Yang, and S. Guha, Appl. Phys. Lett. **85**, 1925 (2004).
[4] G. Yue, B. Yan, J. Yang, and S. Guha, Appl. Phys. Lett. **86,** 092103 (2005).
[5] G. Yue, B. Yan, J. Yang, and S. Guha, J. Appl. Phys. **98**, 074902 (2005).
[6] G. Yue, B. Yan, G. Ganguly, J. Yang, and S. Guha, Appl. Phys. Lett. **88**, 263507 (2006).
[7] B. Yan, G. Yue, J. Yang, S. Guha, D.L. Williamson, D. Han, and C.-S. Jiang, Appl. Phys. Lett. **85**, 1955 (2004).
[8] T. Dylla, F. Finger, E. A. Schiff, App. Phys. Lett. **87**, 032103 (2005).

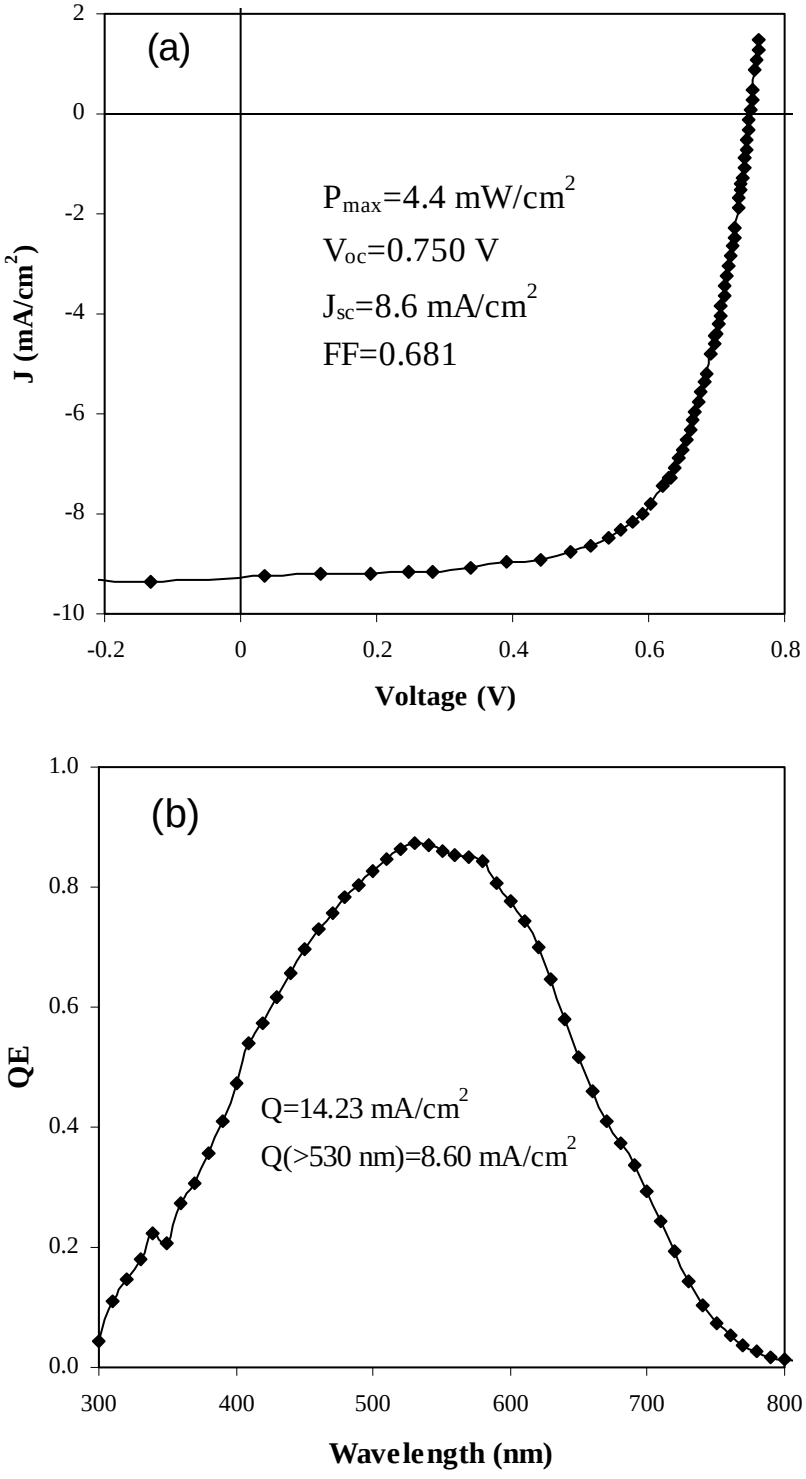

Figure 5. (a) *J-V* characteristics measured under AM1.5 with a 530 nm cut-on filter; and (b) QE spectrum of the best a-SiGe:H middle cells made at 10 Å/s using MVHF.

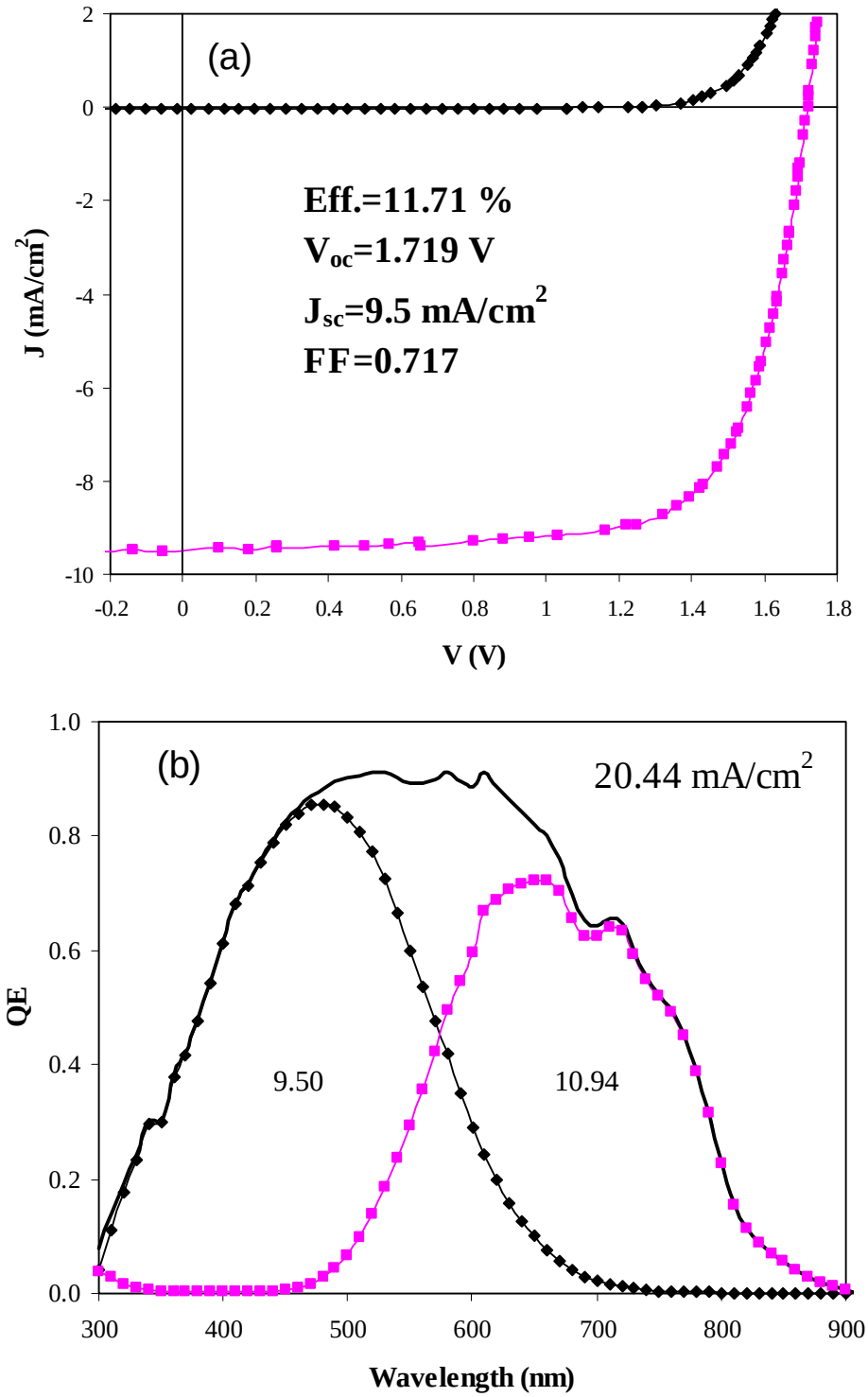

Figure 6. (a) *J-V* characteristics and (b) QE spectrum of an a-Si:H/a-SiGe:H double-junction cells made at 10 Å/s using MVHF.